III International Conference on Particle-based Methods – Fundamentals and Applications
PARTICLES 2013
M. Bischoff, E. Oñate, D.R.J. Owen, E. Ramm & P. Wriggers (Eds)

THE INTRODUCTION OF A BI-ADAPTIVE SMOOTHED PARTICLE HYDRODYNAMICS FORMULATION BENEFICIAL FOR MACHINING PROCESS SIMULATIONS

Fabian Spreng, Alexandra Mueller and Peter Eberhard

Institute of Engineering and Computational Mechanics
University of Stuttgart
Pfaffenwaldring 9, 70569 Stuttgart, Germany
[fabian.spreng, alexandra.mueller, peter.eberhard]@itm.uni-stuttgart.de
www.itm.uni-stuttgart.de

Key words: Machining, Simulation, SPH, ASPH, Adaptivity, Refinement

Abstract. Machining is one of the most important industrial production processes and, therefore, it is of great interest to have a tool suitable to describe the behavior of a real machined workpiece in a simulation. Due to its meshless nature, the Smoothed Particle Hydrodynamics (SPH) method is a quite promising, but frequently not well known alternative to mesh-based techniques, with the Finite Element Method leading the way, when simulating cutting processes. In order to demonstrate this, we present a broad variety of simulation results generated by our enhanced, bi-adaptive SPH cutting algorithm and evaluate them with respect to experimental data. But not only the final results, also the way how to extend the basic SPH code for solids to two adaptive components in order to meet the special requirements demanded by the cutting scenario, the ASPH extension and a newly developed refinement algorithm, is presented.

1 INTRODUCTION

Without any doubt, mesh-based simulation techniques, especially the Finite Element Method (FEM) and its derivatives, are very powerful tools in engineering science. However, when it comes to applications characterized by a highly dynamic or topology changing behavior as well as large deformations of the initial configuration, e.g. machining processes, these tools suffer from several drawbacks due to their mesh-based nature. In contrast to this, meshless methods are a promising alternative in this context, not being limited by an underlying mesh. But also the meshless simulation techniques, for example the Smoothed Particle Hydrodynamics (SPH) method presented in [1], do not provide an out-of-the-box solution to problems of the mentioned type. In order to obtain a simulation setup suitable for such applications, the original SPH method has to be extended. As the first of the two adaptive components of our simulation code, the so-called ASPH extension

introduced in [3] is presented. The ASPH algorithm adapts the interaction range of the SPH particles according to the deformation of the material. Besides the ASPH formulation, a local refinement algorithm is integrated into our code in order to improve the accuracy of the simulation results while reducing the necessary computational expense at the same time.

For validation purposes, we compare the results obtained from an ordinary and a notched tensile test specimen as well as a bending test while using the presented bi-adaptive SPH method with analytical solutions as well as experimental data. Finally, we demonstrate that the employed SPH formulation is capable of reproducing the behavior of a real processed workpiece observed in experiments by analyzing the simulation results in terms of chip morphology, stress distribution as well as cutting forces.

2 SMOOTHED PARTICLE HYDRODYNAMICS

The SPH simulation technique was originally developed from 1977 onwards to simulate phenomena in astrophysics [1] but, basically, it is an universal meshless spatial discretization method leading to a conversion of partial differential equations in time and space into ordinary differential equations in time, which can be treated with common integration schemes. When applying the SPH method to the simulation of solid matter, it replaces the considered continuum domain with a set of particles, i.e. the discretization points, and evaluates the field quantities of the material, such as velocity, density and stress, at these points. These discrete values are then smoothed in space over a support area depending on the so-called smoothing length h to approximate the spatial functions in the partial differential equations.

In addition to the modifications presented in this paper, we have extended the basic formulation given in [1] to include heat dissipation and conduction as well as the purely empirical Johnson-Cook plasticity model along with the related damage model, which are discussed in detail in [2].

3 ADAPTIVE SMOOTHED PARTICLE HYDRODYNAMICS

When using a constant value for the smoothing length h throughout a simulation for problems showing large deformations of the modeled structure, a possible increase in the distance between adjacent particles can lead to a decrease in the number of neighbors located within the smoothing area resulting, sooner or later, in a numerically induced fracture. To overcome this methodological limitation of the SPH method, the ASPH extension [3] can be introduced.

3.1 Algorithm used for the adaption of the smoothing length

To ensure that the damage behavior of the simulated material is, even in case of large strain values, controlled exclusively by an employed fracture model, the scalar smoothing length h has to be adjusted in accordance to the deformation of the observed structure.

For this purpose, the ASPH algorithm uses the normalized coordinate $\eta_{\mathrm{ij}} = |\boldsymbol{r}_{\mathrm{i}} - \boldsymbol{r}_{\mathrm{j}}|/h_{\mathrm{i}}$, where the numerator of this expression represents the distance between particles i and j, to calculate an average distance of the reference particle i to all of its neighbors based on the relation

$$\Psi_{\mathrm{i}} = \left(\sum_{\mathrm{j}} W\left(\eta_{\mathrm{ij}}\right) \right)^{1/q} , \tag{1}$$

where q denotes the dimensionality of the system and the kernel function W is used to weight the influence of each of the pairs of particles on Ψ_{i} in relation to the overall distribution of pairs over the entire smoothing area. Then, in a next step, a table mapping the calculated value for Ψ_{i} onto the effective number of nodes per smoothing scale $n_{\mathrm{h,i}}$, which is defined as the ratio of the smoothing scale to the initial particle spacing, is set up. Using the normalized coordinate η_{ij} to describe the distance between the neighboring particles i and j allows to employ the same sample table for all particles being part of a simulation independently of the individual smoothing length h_{i}. Having specified the target value $n_{\mathrm{h,i}}^{\mathrm{target}}$, the ratio $s_{\mathrm{i}} = n_{\mathrm{h,i}}^{\mathrm{target}}/n_{\mathrm{h,i}}$, which provides the basis for the adaption of the smoothing scale, can be computed. In contrast to the original algorithm introduced in [3], we do not choose a specific value for $n_{\mathrm{h}}^{\mathrm{target}}$ for all ASPH particles forming the model shape in advance, but calculate the initial effective number of nodes per smoothing scale for each particle in a preprocessing operation to be used as $n_{\mathrm{h,i}}^{\mathrm{target}}$ in order to avoid issues resulting from an abruptly jumping smoothing scale h_{i}. For this reason, the nonsurface particles of a specimen show the highest value of $n_{\mathrm{h,i}}^{\mathrm{target}}$, while the number of neighbors decreases the closer the particle is situated to a corner. That way, the ASPH formulation becomes more flexible and convenient if a user wants to perform simulations without using any of the available methods intending to correct the asymmetry of the support area of particles located near the surface of an SPH model.

Once the value for $n_{\mathrm{h,i}}$ for the current time step has been determined and the target value $n_{\mathrm{h,i}}^{\mathrm{target}}$ has been specified, a variable a_{i} is defined following the relation

$$a_{\mathrm{i}} = \begin{cases} 0.4\left(1 + s_{\mathrm{i}}^2\right) & \text{if } s_{\mathrm{i}} < 1 \\ 0.4\left(1 + s_{\mathrm{i}}^{-3}\right) & \text{otherwise} \end{cases} , \tag{2}$$

which is used to adapt the smoothing length h_{i} of each particle according to the equation

$$h_{\mathrm{i}}^{\mathrm{new}} = \left(1 - a_{\mathrm{i}} + a_{\mathrm{i}} s_{\mathrm{i}}\right) h_{\mathrm{i}}^{\mathrm{old}} . \tag{3}$$

A comparison of the results obtained when simulating the standardized test setup of a tensile specimen with and without the ASPH extension is drawn in the following section.

3.2 Tensile specimen

The uniaxial tensile test is one of the most basic experimental setups conducted to investigate the elastic, the plastic and the fracture behavior of real solid material and is,

for this reason, also suitable for a comparison with simulation data. In this work, a regular lattice with quadratic cells of SPH and ASPH particles, respectively, serves as a basis for the two-dimensional model of an ordinary flat tensile specimen. The left edge of the specimen is fixed, while the right one is driven with a constant velocity in such a way that the simulated tensile specimen structure experiences an invariable elongation rate level throughout the entire simulation. To the particles located within the measuring area an initial velocity is assigned according to their relative distance from the grip sections. That way, a linear velocity field is established in order to avoid having shock waves running from one end of the specimen to the other resulting in a noisy stress-strain-curve.

The relationships between stress and strain found when employing the different introduced SPH formulations on the simulation of a flat tensile specimen made of C45E while using approximately 10 000 particles for the discretization of its gauge section with an initial length of $l_0 = 0.05 \cdot 10^{-2}\,\mathrm{m}$ and a width of $b = 1.25 \cdot 10^{-2}\,\mathrm{m}$ are shown in Fig. 1(a). As can be clearly seen, both the stress-strain curve found for the SPH simulation with a constant smoothing length as well as the one obtained with the ASPH model take the same elastic and plastic path up to the point when the tensile specimen simulated with the unmodified SPH method shows a loss of influence between neighboring particles and, thus, a numerical fracture can be observed. At this point, the SPH particles located within the area showing the largest value of strain have too few neighbors in the stretching direction and, as a consequence of this, become decoupled from each other. Running the identical simulation setup as done in case of the standard SPH algorithm with the ASPH method leads to a fairly different, but expected behavior. With an increase in the elongation of the tensile specimen, the distance between neighboring particles is increased, too, and, hence, the smoothing length h is adapted accordingly. As a result, the number of neighboring particles located within the smoothing area of the ASPH particles remains the same until the end of the simulation and the stress-strain curve of the ASPH simulation follows the perfectly plastic path up to a strain value of $\varepsilon = 0.15$. As expected from a theoretical point of view, the ASPH model shows the same increase in the smoothing length h_i all across the measuring range within the elastic region, whereas within the plastic region the highest level of adaption can be found for the areas of highest strain as shown in Fig. 1(b).

In addition to the ASPH algorithm, a density-based criterion for an adaption of the smoothing length h_i, which is often used in case of fluid simulations, should be evaluated concerning its applicability to avoid the issue of numerical fracturing for simulations including solid material. The formulation presented in [4] relates the smoothing length of a particle to its density ρ_i according to

$$h_\mathrm{i} \propto \left(\frac{1}{\rho_\mathrm{i}}\right)^{1/q} . \tag{4}$$

As also shown in [4], the time-dependent evolution of the smoothing scale h_i can be described following

$$\frac{\mathrm{d}h_\mathrm{i}}{\mathrm{d}t} = -\frac{h_\mathrm{i}}{q\rho_\mathrm{i}}\frac{\mathrm{d}\rho_\mathrm{i}}{\mathrm{d}t} . \tag{5}$$

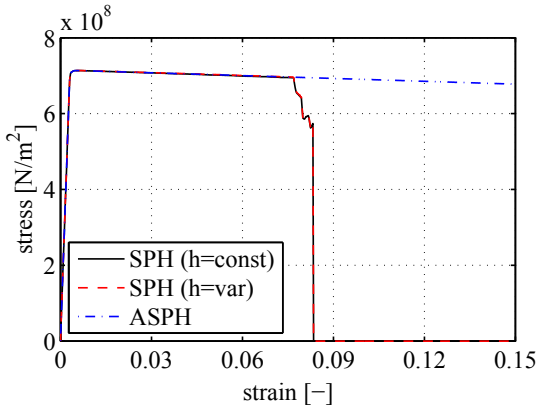

(a) Stress-strain curves obtained when employing different formulations for a variation of the smoothing length h

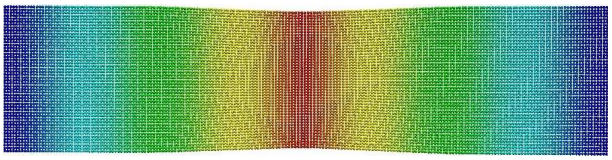

(b) ASPH model of the tensile specimen showing the value of the smoothing length h_i (red: high h_i; blue: low h_i)

Figure 1: Simulation results obtained for the ordinary tensile specimen

Since for solid material the variation in the density is much smaller compared to the one observed for a fluid, the smoothing length h is adapted only to a small degree and, thus, a numerical fracture occurs in case of the tensile specimen at about the same strain level as it does when using the unmodified SPH method, Fig. 1(a). Therefore, density-based methods, like the one introduced in [4], are not really suitable for simulations involving solid matter.

4 ADAPTIVE REFINEMENT

Another way to prevent numerical fracturing and to increase the quality of the simulation results is to insert additional discretization points, i.e. particles, in critical areas. These new particles are placed in a way to fill numerical gaps in the material and to cause least additional strain.

4.1 Particle placement and refinement criteria

The adaptive refinement approach presented in this paper follows the procedure introduced in [5]. In a first step, it is decided whether an existing particle is to be refined at all. If so, it is then split into several smaller particles according to a given refinement pattern. Most of the values of these new particles are interpolated from the ones of the surrounding particles via SPH interpolation, only a few are taken directly from the original particle due to conservation aspects.

There are many ways to place the newly created particles. As a cubical grid is often used as an initial setup for arranging the particles in SPH simulations, we also chose a refinement pattern that retains the initial configuration. For this purpose, it splits the original particle, in case of a two-dimensional simulation, into four smaller ones placed on

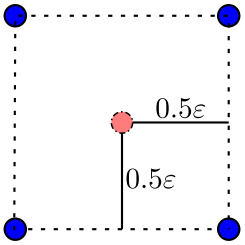

x	1/2	1/2	−1/2	−1/2
y	1/2	−1/2	−1/2	1/2

Figure 2: Two-dimensional cubical refinement pattern and relative particle positions in terms of ε.

the corners of a cube with a length of the edge of ε, as depicted in Fig. 2. Note that the original particle is removed when following this strategy and its position stays vacant.

After having determined the positions of the additional particles, their masses have to be specified. The simplest choice is to distribute the mass of the original particle equally among the new ones. However, this choice pays no regard to the original density field of the simulated material. Therefore, [5] proposes a mass distribution that introduces the least disturbance in the smoothed density field, which is defined as

$$\mathcal{E} := \int_\Omega \left(m_\mathrm{i} W(\boldsymbol{x}_\mathrm{i} - \boldsymbol{x}, h_\mathrm{i}) - \sum_\mathrm{j} m_\mathrm{j} W(\boldsymbol{x}_\mathrm{j} - \boldsymbol{x}, h_\mathrm{j}) \right)^2 \mathrm{d}\boldsymbol{x} \ , \tag{6}$$

where i denotes the original particle and j the new ones, with the corresponding positions $\boldsymbol{x}_\mathrm{i}$ and $\boldsymbol{x}_\mathrm{j}$ and smoothing lengths h_i and h_j, respectively. If the new particle masses are rewritten as $m_\mathrm{j} = \lambda_\mathrm{j} m_\mathrm{i}$, with $\sum_\mathrm{j} \lambda_\mathrm{j} = 1$ to give conservation of mass, (6) yields

$$\mathcal{E} = m_\mathrm{i}^2 \left(C - 2\boldsymbol{\lambda}^\mathrm{T} \boldsymbol{b} + \boldsymbol{\lambda}^\mathrm{T} \boldsymbol{A} \boldsymbol{\lambda} \right) \tag{7}$$

with

$$C = \int_\Omega W_\mathrm{i}^2(\boldsymbol{x}, h_\mathrm{i}) \mathrm{d}\boldsymbol{x} \ , \ \ b_\mathrm{s} = \int_\Omega W_\mathrm{i}(\boldsymbol{x}, h_\mathrm{i}) W_\mathrm{s}(\boldsymbol{x}, h_\mathrm{s}) \mathrm{d}\boldsymbol{x} \text{ and } A_\mathrm{rs} = \int_\Omega W_\mathrm{r}(\boldsymbol{x}, h_\mathrm{r}) W_\mathrm{s}(\boldsymbol{x}, h_\mathrm{s}) \mathrm{d}\boldsymbol{x} \ .$$

With the choice $h_\mathrm{j} = \alpha h_\mathrm{i}$ for all particles j, (7) can be rewritten as

$$\mathcal{E} = \frac{m_\mathrm{i}^2}{h_\mathrm{i}^q} \left(\bar{C} - 2\boldsymbol{\lambda}^\mathrm{T} \bar{\boldsymbol{b}} + \boldsymbol{\lambda}^\mathrm{T} \bar{\boldsymbol{A}} \boldsymbol{\lambda} \right) \tag{8}$$

with

$$\bar{C} = \int_\Omega W_\mathrm{i}^2(\boldsymbol{x}, 1) \mathrm{d}\boldsymbol{x} \ , \ \ \bar{b}_\mathrm{s} = \int_\Omega W_\mathrm{i}(\boldsymbol{x}, 1) W_\mathrm{s}(\boldsymbol{x}, \alpha) \mathrm{d}\boldsymbol{x} \text{ and } \bar{A}_\mathrm{rs} = \frac{1}{\alpha^q} \int_\Omega W_\mathrm{r}(\boldsymbol{x}, \alpha) W_\mathrm{s}(\boldsymbol{x}, \alpha) \mathrm{d}\boldsymbol{x} \ .$$

For further details, see [5]. With $\sum_\mathrm{j} \lambda_\mathrm{j} = 1$ the optimization problem reads

$$\min_{\boldsymbol{\lambda}} \left(\bar{C} - 2\boldsymbol{\lambda}^\mathrm{T} \bar{\boldsymbol{b}} + \boldsymbol{\lambda}^\mathrm{T} \bar{\boldsymbol{A}} \boldsymbol{\lambda} \right) \ . \tag{9}$$

In general, a solution exists as $\bar{\boldsymbol{A}}$ is symmetric and positive definite, but it may also result in unwanted and unphysical negative particle masses. The solution depends on the choices for the dispersion ε, the smoothing length scale α as well as the kernel function. This approach makes the solution independent from the initial particle distance, mass and smoothing length and, therefore, it has to be evaluated only once using the unity mass and length at the beginning of the simulation, which takes little additional computation time. During the simulation, the pattern can be adapted by scaling it with the actual values of the state variables of the original particle.

Up to now, the positions, masses and smoothing lengths of the new particles have been specified, the other properties, such as the densities and the velocities, need to be set, too. While most state variables, as for example the densities, are calculated via SPH interpolation from the original particles, the velocities are set to the ones of the original particles to achieve a conservation of linear and angular momentum as well as kinetic energy. Choosing $\boldsymbol{v}_\mathrm{j} = \boldsymbol{v}_\mathrm{i}$ for all particles j is the only way to ensure exact conservation.

Having specified how to refine a specific particle, the important question is when to refine a particle at all. One or several suitable refinement criteria need to be chosen for each simulation setup, e.g. using single particle values, field gradients over the neighborhood or numerical data, such as the number of neighbors.

4.2 Bending specimen

As an alternative to the ASPH extension, the refinement algorithm is suitable to avoid a numerical fracture when simulating solid structures experiencing large deformations. This is demonstrated by taking the example of a cantilevered beam. For this purpose, the ordinary tensile test presented in Section 3.2 is modified, applying a constant force acting in lateral direction to the right edge of the specimen. That way, the resulting bending moment increases linearly along the longitudinal axis of the beam model and reaches its maximum value next to the left edge of the specimen, which has been fixed in space. Hence, the longitudinal stress depicted in Fig. 3 follows, except for the grip areas, a linear distribution and, as expected, the maximum stress level can be found for the surface areas of the specimen. The longitudinal stress values of the SPH particles located within the compressive region show the same absolute values as the ones of the corresponding particles located within the tensile region, but of negative sign, and one can find a zero stress level along the neutral axis of the bending specimen.

To prevent numerical fracturing by increasing the number of particles through refinement, it is necessary to choose a suitable criterion. In case of the cantilevered beam, a stress-based criterion would lead to a refinement not only of the tensile, but also of the compressive region, for which no numerical fracture will be observed. That way, the number of particles and with it the computation time is increased immensely. Therefore, we employ a strain-based refinement criterion that ensures that only the tensile part of the specimen is refined. The chosen refinement pattern is the cubical one, see Fig. 2, with $\varepsilon = 0.5$ and $\alpha = 1.0$ to retain the cubical pattern of the initial setup. The overall number

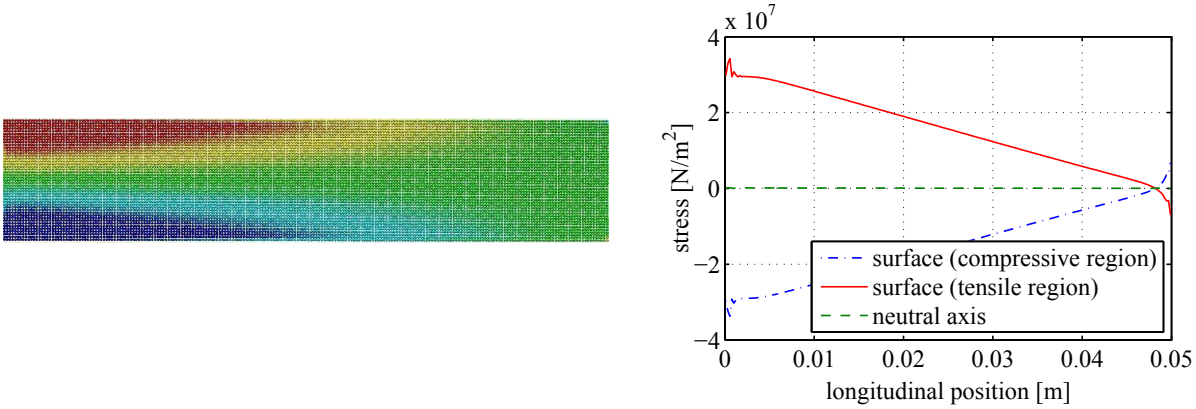

(a) Entire specimen (red: high stress; blue: low stress)

(b) Specific regions

Figure 3: Distribution of the longitudinal stress found for the model of a cantilevered beam

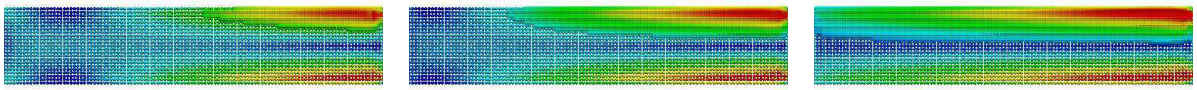

Figure 4: Different stages from the refinement of the bending specimen (red: high stress; blue: low stress)

of particles at the beginning is about 2 800. As expected, when applying the lateral force to the right edge of the specimen in downward direction, the right end of the beam is pressed downwards and the highest strain value can be found at the top right corner of the specimen, spreading more and more to the left one over time. As can be seen in Fig. 4, the particle refinement follows this development, resulting in a completely refined upper half of the beam with an increased concentration of particles at the end of the simulation.

4.3 Notched tensile specimen

Next, the focus is laid on the possibility to improve the accuracy of the simulation results by refining specific areas of the model, e.g. areas that show high gradients in stress. As a fairly inhomogeneous stress distribution can be found in case of a notched tensile specimen, we use this simulation example as evaluation setup for the introduced refinement algorithm. A regular lattice with quadratic cells of SPH particles serves as a basis for the two-dimensional model of a flat double-edge notched tensile specimen with a width of $1 \cdot 10^{-2}$ m and an initial length of $1.34 \cdot 10^{-2}$ m. Halfway up the length of the created geometry round notches with a radius r of $1.5 \cdot 10^{-3}$ m and an offset of $2 \cdot 10^{-4}$ m from the outer edge are introduced on both sides of the specimen. An initial particle spacing of $2.3 \cdot 10^{-3}$ m is used for the discretization of the refined SPH simulation, leading to an overall number of particles of about 2 700 at the beginning of the simulation. The

chosen refinement criterion is stress-based combined with a restriction on the particle position. Thus, those particles are refined that experience high stresses and are situated inside a circular area around the center of the specimen. The cubical refinement pattern as introduced in Fig. 2 with $\varepsilon = 0.5$ and $\alpha = 1.0$ is employed. For comparison, an unrefined SPH simulation with an initial particle spacing of $1.15 \cdot 10^{-3}$ m is used, leading to an overall number of particles of about 10 000. As it is hardly possible to determine the stress distribution found for a notched tensile specimen in an analytical way, two simulation-based references are used for comparing the results computed by the SPH method, a simulation of a notched tensile test performed by the Finite Element program ADINA and one employing the Discrete Element Method (DEM) [6].

As can be clearly seen when analyzing the distribution of the von Mises equivalent stress given in Fig. 5, the results obtained when employing the four different simulation techniques on the notched tensile scenario are in good agreement and, thus, the SPH refinement is able to reproduce the stress distribution observable for a real notched specimen. According to that, the maximum value of the von Mises stress can be found right at the roots of the two notches, whereas the level of equivalent stress decreases when following the paths from the roots to the centerline of the tensile specimen. Furthermore, the von Mises stress attains lower and lower values along the notch radii, starting with a high stress level at the roots and showing stress-free areas next to the outer surface of the specimen. The elliptic section of the model characterized by a high magnitude of equivalent stress and aligned with its minor axis along the ligament line that can be identified when examining the three reference solutions is also obvious in case of the refined SPH notched tensile test.

The areas of highest stress and, according to that, of highest strain are also the areas where the simulated material first experiences an increase in the discretization level. Therefore, as shown in Fig. 6, the refinement starts at the roots of the notches and spreads along the elliptic area of high equivalent stress until most of the circular area is refined.

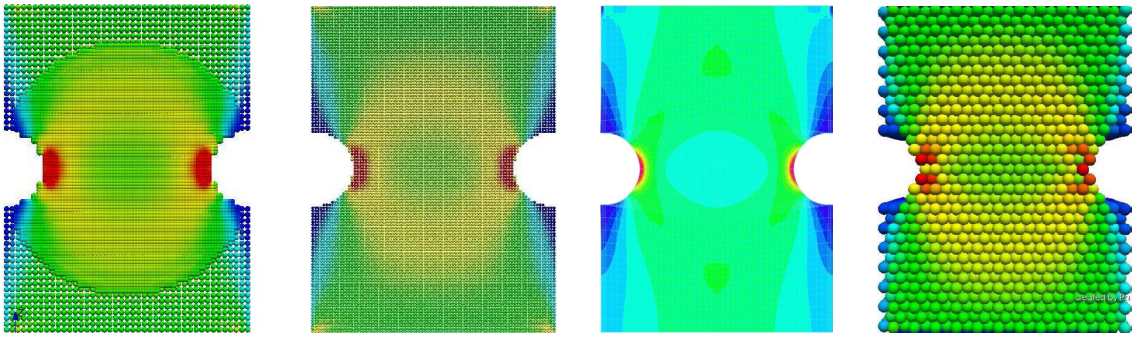

(a) refined SPH (b) SPH (c) FEM (d) DEM

Figure 5: Distribution of the von Mises stress found for the model of a double-edge notched tensile specimen when using different simulation methods (red: high stress; blue: low stress)

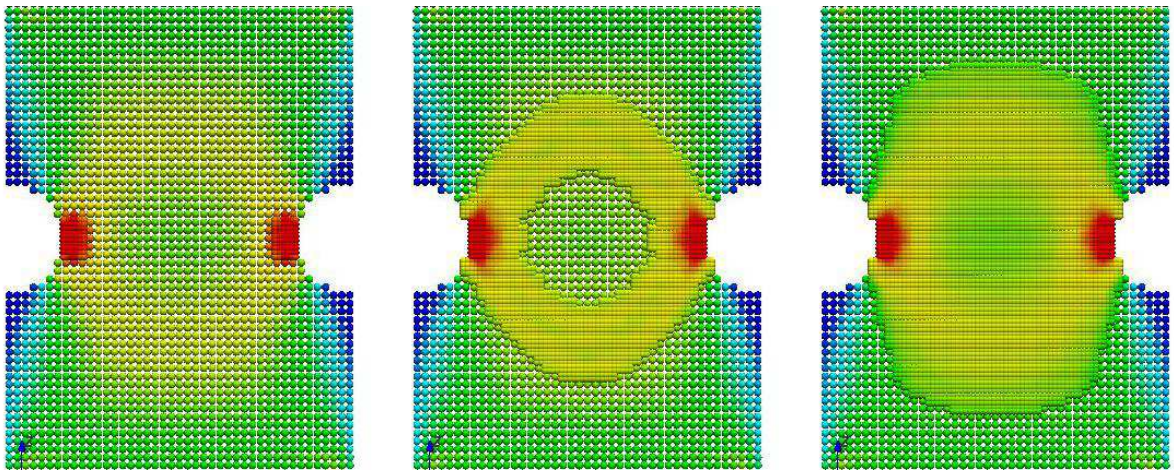

Figure 6: Selected times from the refinement of the notched SPH tensile specimen (red: high stress; blue: low stress)

Small parts of the refinement circle located close to the outer surfaces of the specimen remain unchanged, as the von Mises stress stays below the specified refinement threshold value for these regions.

5 CUTTING SIMULATION

The presented enhanced SPH formulation is also applicable to the simulation of cutting processes leading to results similar to the ones obtained from experiments. The orthogonal cutting setup represents an elementary cutting process where the motion of the tool is perpendicular to the cutting edge. When assuming a sufficiently large width of cut compared to the chosen depth of cut, a two-dimensional state of stress can be assumed in the workpiece and the machining process becomes a planar problem. Due to the two-dimensional state of stress, two force components acting on the tool can be identified. They are called cutting force, which acts in the feed direction, and passive force, acting perpendicular to the feed direction [7].

For the model of the cutting specimen the ASPH particles are arranged according to a regular quadratic lattice with an initial distance of about $3 \cdot 10^{-4}\,\mathrm{m}$. To prevent the workpiece model from following an unconstrained translational motion, five additional rows of particles that are fixed in space are attached to the bottom of the specimen. The material used for the experimental investigations and, thus, also for the cutting simulation is steel C45E. For the calculation of the particle forces resulting from the interaction with the cutting tool the penalty approach described in [2] is deployed. The behavior of the cutting model that can be observed when using the extended SPH cutting algorithm is discussed hereinafter.

When the cutting of material takes place, the distribution of the von Mises stress shown in Fig. 7(a), with red meaning high stress and blue indicating low stress, can be found.

The highest level of stress appears next to the tip of the tool where the separation of material happens. This zone showing a high magnitude of stress is surrounded by a zone of mid-level stress color coded in yellow and green. Both the particle layers located at some distance from the tool tip as well as the parts of the material that form the chip show low values of von Mises stress indicated by the blue color of the ASPH particles. In similarity to the experimental results, a continuous chip is separated from the remaining workpiece material in the cutting simulation. In this context, it is important to remember that the particles shown in Fig. 7(a) only illustrate the interpolation points where the equations of the underlying continuum model are evaluated, and not domains of material.

In order to assess the enhanced SPH method with regard to its applicability to model cutting processes, an experimental reference is used, comparing the forces acting for a depth of cut of 10^{-3} m with the simulated ones. When examining the results given in Fig. 7(b), the cutting force obtained from the experimental setup shows a steep increase once the tool hits the workpiece until a steady state is reached. The simulated curve is characterized by a steep rise too, followed by an overshoot and an oscillation about a steady state at about the same level observed in case of the experimental results, but showing a slightly wider range of variation in the cutting force. Except for the transition area between the steep increase just after the impact has happened and the steady state, the results of the presented cutting simulation are in good agreement with the behavior identified for the experimental specimen. In addition to the cutting force depicted in Fig. 7(b), one can find such high quality of reproduction also for the passive force.

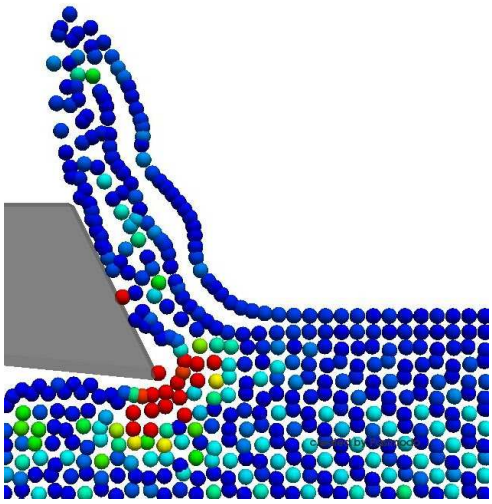

(a) Distribution of the von Mises stress (red: high stress; blue: low stress)

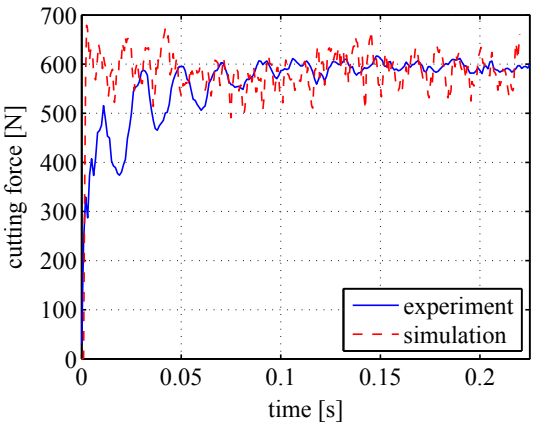

(b) Comparison of the experimental and the simulated cutting force

Figure 7: Simulation results obtained for the orthogonal cutting specimen when using the enhanced SPH cutting process model

6 CONCLUSIONS

Taking the enhanced SPH particle method for solid bodies presented in [2] as a starting point, we integrated two adaptive techniques into our simulation environment in order to be able to model the process of cutting metal in a realistic way. We extended our SPH code, in a first step, to a slightly modified version of the ASPH algorithm introduced in [3]. By adapting the smoothing length accordingly, the number of neighbors is kept constant and a numerical fracture is avoided, which was shown in the context of an ordinary tensile test simulation. In a further step towards an enhanced cutting formulation, we extended the SPH method for solids to a newly developed refinement technique based on the one presented in [5], where additional particles are inserted in certain areas. The results obtained from a bending and a notched tensile test were compared with analytical solutions as well as results generated with other simulation methods. Finally, we showed that the enhanced, bi-adaptive SPH formulation is capable of reproducing the behavior of a real processed workpiece made of steel C45E. Future investigations will lay the focus on the vibration behavior of the overall cutting system, the temperature distribution within the workpiece and comparisons on the cutting force when applying different depths of cut.

REFERENCES

[1] Monaghan, J.J. Smoothed Particle Hydrodynamics. *Reports on Progress in Physics* (2005) **68**:1703–1759.

[2] Spreng, F.; Eberhard, P. and Fleissner, F. An approach for the coupled simulation of machining processes using Multibody System and Smoothed Particle Hydrodynamics algorithms. *Theoretical and Applied Mechanical Letters* (2013) **3**:013005-1–7.

[3] Owen, J.M. ASPH modeling of material damage and failure. *Proceedings of the 5th International SPHERIC Workshop* (2010) 297–304.

[4] Price, D.J. *Magnetic fields in astrophysics*. Ph.D. thesis, University of Cambridge (2004).

[5] Feldman, J. *Dynamic refinement and boundary contact forces in Smoothed Particle Hydrodynamics with applications in fluid flow problems*. Ph.D. thesis, University of Wales, Swansea (2006).

[6] Cundall, P.A. and Strack, O.D.L. A discrete numerical model for granular assemblies. *Géotechnique* (1979) **29**:47–65.

[7] Gaugele, T. and Eberhard, P. Simulation of cutting processes using mesh-free Lagrangian particle methods. *Computational Mechanics* (2013) **51**:261–278.